Molecular radiative transport. III. Experimental intensity decays

Eduardo J. Nunes Pereira[a)]
*Centro de Química-Física Molecular, Instituto Superior Técnico, 1096 Lisboa Codex, Portugal
and Universidade do Minho, Escola de Ciências, Departamento de Física, 4709 Braga Codex, Portugal*

Mário N. Berberan-Santos and Aleksandre Fedorov
Centro de Química-Física Molecular, Instituto Superior Técnico, 1096 Lisboa Codex, Portugal

Michel Vincent and Jacques Gallay
*LURE, Laboratoire pour l'Utilisation du Rayonnement Electromagnétique, Université Paris-Sud,
Bâtiment 209D, 91405 Orsay Cedex, France*

José M. G. Martinho
Centro de Química-Física Molecular, Instituto Superior Técnico, 1096 Lisboa Codex, Portugal

A critical experimental test of a previously developed theory of molecular radiative transport is described. It is concluded that the theory gives an accurate description of the effect of radiative transport on fluorescence observables. The numerical coefficients of the fluorescence decay are computed from a Monte Carlo integration procedure that mimics the photon trajectories inside a realistic sample cell, and is carried out only using known molecular and geometrical parameters. The predicted parameters are confronted with the experimental observables accessible in a typical single-photon timing experiment, rhodamine 101 in ethanol being the system studied. The theoretical predictions quantitatively describe the effects of concentration and excitation and emission wavelengths experimentally observed in optical dense nondiffusing media for the two most common geometric arrangements: front-face and right-angle detection. It is shown that radiative transport leads to spatially heterogeneous fluorescence kinetics, as a direct consequence of the existence of a spatial distribution function of electronic excitation inside the sample cell. The agreement between theory and experimental results is good, with the average decay times predicted within $\simeq 3\%$ accuracy for front-face detection. © *1999 American Institute of Physics.*
[S0021-9606(99)00202-0]

I. INTRODUCTION

Radiative transfer, i.e., the transfer of energy mediated by real (as opposed to virtual) photons, is ubiquitous in nature. For instance, the first step of photosynthesis consists of the radiative transfer from the sun's photosphere to the chlorophyll molecules of green plant leafs. Donor and acceptor are, in this case, 150 000 000 km apart, and the process takes 8 min to be completed. Radiative transfer is also of importance in astrophysics, plasmas and in atomic and molecular luminescence, and plays a significant role in solar concentrators, discharge and fluorescent lamps, scintillation counters and lasers.

The type of radiative transfer to be discussed in this work consists of the emission of a photon by an electronically excited molecule, with subsequent absorption by an identical ground state molecule. It involves distances much smaller than those of the above example, and consequently occurs on much shorter time scales, usually determined by molecular excited state lifetimes and not by photon propagation times. In assemblies of like atoms or molecules the photons emitted by electronically excited species may be reabsorbed and re-emitted several times before they can leave the sample. This phenomenon is indifferently known as radiation imprisonment, radiative migration, radiative trapping, or radiative transport (in this latter case, transport is used to differentiate it from the case of *transfer* between unlike molecules). Its importance depends on many factors: extent of spectral overlap between absorption and emission, fluorescence quantum yield, absorption coefficients in the overlap region, concentration, sample cell size and shape, excitation and detection geometries, etc. When present, this process affects the fluorescence decays and spectra, as well as the fluorescence anisotropy.

In part I of this series,[1] a stochastic theory of radiative transport allowing the calculation of all observables from known parameters was presented. This theory was subsequently refined and extended to cases where nonradiative transport operates in parallel with radiative transport.[2] In part II,[3] a detailed computation of the coefficients of the derived laws was made according to a Monte Carlo (MC) simulation procedure. This simulation allowed, for the first time, the accurate calculation of the effect of radiative transport on fluorescence intensity and anisotropy decays, time-resolved and steady-state spectra, as well as on the values of the macroscopic quantum yield and steady-state anisotropy. In the present work, we carry out a critical experimental test of the proposed theory for molecular radiative transport for the sys-

---
[a)]Electronic mail: epereira@fisica.uminho.pt

tem rhodamine 101 in ethanol. We compare the experimental time-resolved emission with the MC predictions built upon the basic theoretical equations derived before for two common excitation/detection geometries: front-face and right-angle.

In Sec. II, we begin by summarizing the scope and assumptions of the developed stochastic theory (Sec. II A), and then present the basic equations for the ensemble delta-pulse fluorescence intensity decay law (Sec. II B). The MC integration of the sought mean escape probabilities is briefly mentioned in Sec. III. Section IV contains experimental details. Section V presents the most important aspects of the data analysis procedures. The agreement of the experimental data with the theoretical predictions is discussed in Sec. VI. The compared parameters are defined in Sec. VI A. In Secs. VI B and VI C, the results obtained for both front-face (Sec. VI B) and right-angle (Sec. VI C) geometries are presented. Finally, Sec. VII summarizes the main conclusions.

II. STOCHASTIC THEORY

A. Scope and assumptions

Let there be excitation of an ensemble of identical molecules by an external source. Part of the emission of the directly excited molecules will be reabsorbed, opening the possibility of radiative transport of the electronic excitation energy, and giving rise to several generations of indirectly excited molecules. The stochastic model for the analysis of the time evolution of the reabsorption-distorted fluorescence emission has been previously presented.[1,2] The assumptions made are the following:[1,3,4] (i) The excitation intensity is low, producing nonsaturating conditions. This allows the calculation of the responses to several excitation modes, including the steady or photostationary state, from the δ-excitation pulse decay law of the molecular ensemble. (ii) The propagation time of re-emitted photons is negligible (compared to the overall retention time inside the cell and to the molecular lifetime τ_0). (iii) Absorption and emission are homogeneously broadened, i.e., a single type of molecule is present. (iv) The molecular emission spectrum is the same for all generations of excited molecules (attainment of thermal equilibrium prior to emission) and independent of the excitation wavelength. Two other approximations are: (v) insignificant molecular diffusion and (vi) insignificant nonradiative transport. The change in the spatial distribution of excited species by molecular diffusion in fluid solutions ($D \simeq 10^{-5}$ cm^2 s^{-1}) is negligible; Nonradiative migration deserves a special comment. Regarding the decay law, the existence of nonradiative transfer hops has no effect on it. In fact, it is well known that a pure nonradiative transport process leaves the decay law unchanged.[5] The combined influence of the radiative and nonradiative mechanisms could in principle induce a change in the decay but only if the spread of the excitation distribution due to nonradiative hops were significant in macroscopic terms. That is not however the case since, by definition, nonradiative hops are performed locally, the resulting excitation spread being usually a few average molecular distances. Nevertheless, the nonradiative mechanism will manifest itself primarily in the anisotropy

emission data of the ensemble. A theoretical treatment of the combined effect of radiative and nonradiative transport on the fluorescence anisotropy was already published.[2] A further consequence of the existence of nonradiative hops is the effective randomization of the orientation of the emitting dipoles, making the additional assumption of isotropic emission appropriate even in rigid media where molecular rotation is hindered.

B. Delta-pulse decay law

Consider a macroscopically homogeneous distribution of identical ground state molecules in a convex but otherwise arbitrary shape enclosure (e.g., a fluorescence cell). Let there be the absorption of an external photon at $t=0$ according to a particular spatial distribution function—$p_1(\mathbf{r})$—given by the application of the Lambert–Beer law along the line corresponding to external excitation. Each individual species excited at time zero will relax to the ground state with a rate constant Γ.

Consider now the time-resolved fluorescence emission for a molecular ensemble created at time $t=0$ by a δ-pulse of essentially monochromatic light. As a consequence of radiative migration, at any time, the ensemble's fluorescence emission results not only from the contribution of directly excited molecules but also from the additional contribution of those created by reabsorption. The probability $p_b(\lambda,t)$ that, between t and $t+dt$, a photon with wavelength λ will hit the enclosure's boundary at a given point $\mathbf{r}_b$ and will thus leave the sample, can be obtained by a sum over all generations of excited molecules by:

$$p_b(\lambda,t) = \sum_{n=1}^{\infty} f_{bn}(\lambda) g_n(t), \tag{1}$$

the individual contribution of each generation being a factorization of $f_{bn}(\lambda)$, the reabsorption dependent probability that a photon with wavelength λ will hit the boundary at point $\mathbf{r}_b$ after exactly n absorption-emission events, and $g_n(t)$, the probability that an nth generation molecule will emit a photon between t and $t+dt$, given that it will emit one. Assuming a negligible photon propagation time, this probability (normalized density function) is given by[1]

$$g_n(t) = \Gamma \frac{(\Gamma t)^{n-1}}{(n-1)!} e^{-\Gamma t}. \tag{2}$$

The escape probability $f_{bn}(\lambda)$ can be computed either considering the whole volume of the enclosure or just the solid angle seen by the detection system. In the absence of radiative transport, the (normalized) fluorescence decay does not depend on the detection direction. However, whenever radiative transport is present, the symmetry of the emitting ensemble is lowered and a complicated positional pattern emerges, where the fluorescence decays become a function of the measuring direction. Because of this, we will formulate the escape probabilities relative to the solid angle subtended by the optical collecting system and add the superscript Ω to emphasize it:

$$f_{bn}^{\Omega}(\lambda) = \frac{1}{4\pi}\,\Phi_0 F(\lambda) \int_{\Omega} [1 - \alpha_b(\mathbf{r},\lambda)] P_n(\mathbf{r}) d\mathbf{r}. \qquad (3)$$

The integration goes over $P_n(\mathbf{r})$, which is the probability that a nth generation photon is emitted at $\mathbf{r}$. Φ_0 is the molecular fluorescence quantum yield and the absorption probability $\alpha_b(\mathbf{r},\lambda)$ is given by

$$\alpha_b(\mathbf{r},\lambda) = \int_0^{|\mathbf{r}_b - \mathbf{r}|} k(\lambda)\exp[-k(\lambda)x]dx, \qquad (4)$$

where $F(\lambda)$ is the (normalized) emission spectrum and $k(\lambda)$ is the optical density of the medium at wavelength λ.

The normalized (i.e., scaled to one for $t=0$) decay can be written as[2]

$$\rho_b^{\Omega}(\lambda,t) = e^{-\Gamma t}\sum_{n=1}^{\infty}\left(\frac{1-\alpha_{bn}(\lambda)}{1-\alpha_{b1}(\lambda)}\right)\left(\prod_{i=1}^{n-1}\bar{\alpha}_i\right)\frac{(k_r t)^{n-1}}{(n-1)!}, \qquad (5)$$

where k_r is the molecular intrinsic radiative decay constant. If one defines $p_n(\mathbf{r})$ as the spatial distribution of the nth generation molecules, the generation dependent mean reabsorption probability can be cast as

$$\alpha_{bn}^{\Omega}(\lambda) = \int_{\Omega}\alpha_b(\mathbf{r},\lambda)p_n(\mathbf{r})d\mathbf{r} \qquad (6)$$

and the product $\prod_{i=1}^{n-1}\bar{\alpha}_i$ is the mean probability of the external excitation giving rise to excited molecules belonging to the nth generation. $\bar{\alpha}_n$ differs from α_{bn}^{Ω} because it quantifies the mean probability that an nth generation photon will be reabsorbed somewhere within the enclosure and must then be given as a double integration over all possible emission wavelengths and reabsorption coordinates.

Equation (5) gives the normalized decay law for one particular emission wavelength and detection solid angle. It is possible to obtain entirely analogous equations for the decays considering both an integration over all space directions and a double integration over space directions and wavelengths.[2] The first case describes the emission detected over the whole 4π solid angle while the second case completely describes the temporal evolution of the excitation in the molecular ensemble. However, from an experimental point of view, the decay is usually recorded at some particular wavelength. Furthermore, unless one uses an integrating sphere, information is limited to the decay at a given boundary point and Eq. (5) is the equation to be used for a comparison of the theoretical predictions with the experimental results.

III. MONTE CARLO SIMULATION

Although the stochastic theory presented above allows the exact computation of the influence of radiative migration on the fluorescence observables, most of the coefficients of the equations derived before are not amenable to analytical form. Given the probabilistic nature of the underlying process of energy migration, a MC integration built upon the basic equations presented is particularly well suited for their numerical evaluation.[3]

Because one can factorize the space and time dependencies of radiative migration, and since the exact time depen-
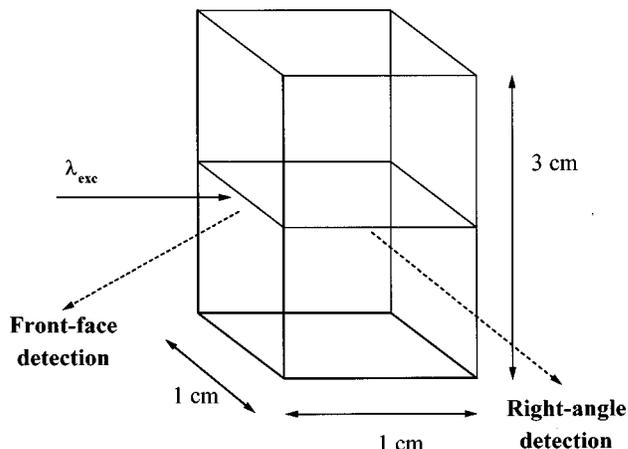

FIG. 1. Tridimensional cell showing the two experimental used detection geometries also reproduced in the MC simulation. The enclosure size and shape correspond to a typical fluorescence cell.

dence is known [Eq. (2)], the simulation procedure is reduced to the generation of the spatial excitation migration trajectories. The goal of the simulation is the computation of the mean escape probabilities [Eq. (3)] which completely defines the predicted decay law.[3]

The MC simulations were implemented as described in part II of this series[3] for a mimic of a conventional $1\times1\times3$ cm fluorescence cell. Two common experimental geometries were considered: front-face detection, usually used to monitor concentrated solutions, and right-angle viewing, the chosen geometry for dilute samples (Fig. 1).

IV. EXPERIMENT

A. System studied

Solutions of rhodamine 101 (Radiant Dyes Chemie, perchlorate salt) in ethanol (Merck UVASOL, min. 99.9%) were used through the work without degassing. Ethanol was acidified with a very small amount ($\simeq 10\ \mu$l per 10 ml solution) of concentrated HCl (min. 37%, Riedel–de Haën) and solution results were always recorded at room temperature (20 ±1 °C). The purpose of the acidification step was to ensure that the chemical species was at all stages the acid form of the dye since it was verified that in pure absolute ethanol an acid-base equilibrium for the dye was effective: for very dilute solutions the basic form was dominant, with the equilibrium shifting towards the acid form with increasing concentration. This behavior is well known for this class of dye molecules.[6,7]

Rhodamine 101 in ethanol is particularly well suited for our goal of providing an experimental test for the theory developed due to the combination of several factors maximizing the importance of radiative transport: high absorption-emission spectral overlap ($\simeq87\%$), high fluorescence quantum yield (89%), and high absorption coefficients in the overlap region (Fig. 2).

B. Fluorescence decays

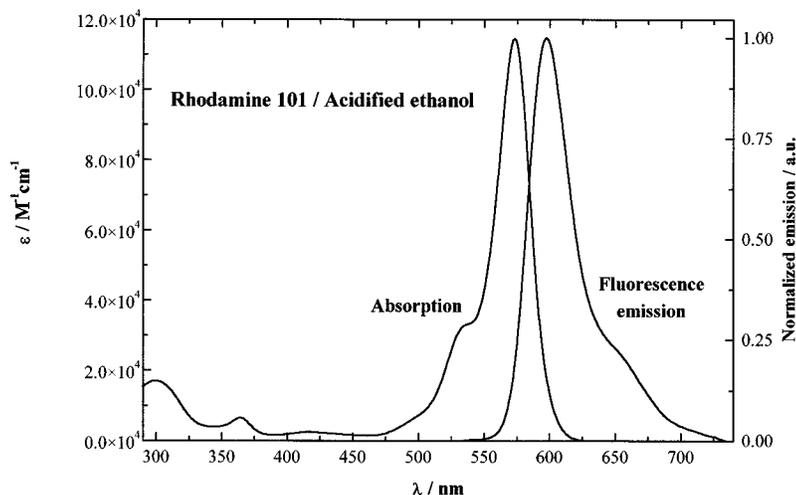Fluorescence decays were measured with the single-photon timing technique (SPT)[8] using a Coherent mode-

FIG. 2. Absorption and fluorescence spectra of rhodamine 101 in acidified ethanol at room temperature. Fluorescence emission for a 5×10^{-7} M solution in right-angle geometry.

locked synchronously pumped dye laser system. An argon–ion laser (Innova 400 using a 468AS mode locker), delivering $\simeq 100$ ps pulses, pumped two identical dye laser Coherent 700 systems, one using rhodamine 6G and the other DCM as the active amplification media. The output of the dye laser is optoacoustically cavity dumped (Coherent 7220) producing pulses of 5–7 ps at a 3.4 MHz repetition rate frequency. The direct output of the dye laser was typically used to make the second harmonic generation (SHG) in an angle-tuned β-barium borate (BBO) crystal and the frequency doubled pulse passed through a Soleil–Babinet compensator to rotate the polarization plane back to the vertical plane. Whenever the fundamental dye laser output was used as the excitation source, the energy density was reduced by an appropriate neutral density filter. The rhodamine 6G and DCM laser dyes allowed a variable excitation wavelength covering the range of about 280–320 nm (SHG) by tuning of a three-plate birefringent filter in the dye laser cavity. Detection was always done by passing the emission through a depolarizer and then through a Jobin–Yvon HR320 monochromator with a grating of 100 lines/mm. Two Hamamatsu photomultipliers were used: a conventional uncooled R3235 photomultiplier and a cooled R2809U-01 microchannel plate. Both were operated under the usual nonpile-up pulse conditions.[10] A total of about 20 000 (right-angle) or 30 000–50 000 (front-face) counts was typically accumulated in the channel of maximum counts. The measurements were made using variable monochromator slits—from 0.5 to about 5 nm—depending on the overall emission intensity and, whenever possible, a visible cutoff filter was used in the detection optics to avoid spurious scattered light on the fluorescence decay. No significant ''wavelength shift'' of the time response of the detection system due to the so-called color effect of the photomultiplier was detected.

The single-photon timing was operated as usual in the reversed configuration,[8] the only additional care being the use of an appropriate delay line and a bias amplifier in order to: (i) have both the start and stop signals originate from the same excitation laser pulse thus minimizing laser jitter and (ii) be able to span the whole useful decay times in as much as possible of the 10 V output range of the time-to-amplitude converter (TAC) in order to reduce the jitter of the measuring

electronics. The electronics were components from Canberra standard nuclear instrumentation modules.

The instrument response function was recorded with a LUDOX scatterer solution sufficiently dilute to preclude multiple scattering. The instrument response function had an effective full width at half maximum (FWHM) of 35 ps (R2809U-01 photomultiplier).

C. Quantum yield efficiency

The fluorescence quantum yield was estimated by the relative method.[9] The ratio of the steady-state fluorescence spectrum area of the unknown quantum efficiency sample to the emission area of a known efficiency reference was used to estimate a fluorescence quantum yield of 0.89 ± 0.05 for the rhodamine 101 solutions. Two different references were used: rhodamine 6G in ethanol with a quantum yield of 88%[10] and cresyl violet in methanol with a quantum yield of 51%.[11] These dyes were chosen in order to have a fluorescence spectrum as close as possible to the rhodamine 101 emission. The solvent refractive index correction (solid angle n^2 factor) was applied whenever cresyl violet was used. The optical density at excitation wavelength of sample and references was matched for solutions of about 10^{-4} M concentration. After that, all solutions were properly diluted so that the steady-state emission could be recorded for very dilute samples (with concentrations always less than 10^{-6} M). Steady-state emission was recorded in a SPEX Fluorolog F112A fluorimeter equipped with a double emission monochromator in a right-angle geometry.

There is still some controversy concerning the value of the fluorescence quantum yield of the rhodamine 101 dye. In early work it was consensual that the fluorescence quantum yield should be close to one.[12] Significantly smaller values are nevertheless found in the literature and in particular our 89% value for the acid form of the dye compares favorably with a recently published value of 92% by Drexhage *et al.*[13] The interpretation of older literature values is also rendered difficult by the fact that sometimes it is not clear from the original data whether the cationic or the zwitterionic form of the dye was considered. The equilibrium between these two forms in ethanol is known to be concentration dependent.

Some results exist for the similar rhodamines B and 19[7] showing that, in ethanol, the acid/cationic form (the dye form considered in the current work) can have a significantly lower emission efficiency than the basic/zwitterionic one.

V. TIME-RESOLVED DECAYS DATA ANALYSIS

The recorded SPT fluorescence decays were analyzed by two different procedures: a modified Levenberg–Marquardt nonlinear least squares (NLLS) algorithm and a maximum entropy method (MEM) procedure. In both approaches a re-iterative fitting and reconvolution algorithm was used. Effort was made to ensure that the data analysis recovered physically significant parameters, as it was found that the analysis of the radiative distorted fluorescence decays is a severely ill-conditioned numerical analysis problem.

A. Nonlinear least squares

Nonlinear least squares were used as a maximum likelihood estimator of the fitted parameters and relied on an implementation of the Marquardt algorithm.[14,15] This method involves solving a sequence of local linear representations of the nonlinear least squares problem. The standard implementation of the algorithm generalizes the method of normal equations to solve the sets of linear equations. This direct solution of the nonlinear least squares problem is rather susceptible to roundoff error. Furthermore, it was found that the normal equations were sometimes very close to singular. In this case, a very small pivot element was found giving rise to fitted parameters with very large magnitudes but delicately (and unstably) balanced to cancel out almost precisely when the fitted function was evaluated. Typically, for generation numbers higher than three, each generation contribution to the overall decay was increasingly (and alternately positive and negative) higher than the contribution of the preceding generation, an unacceptable situation on physical grounds. Given that, although nonlinear, the Marquardt algorithm is reduced to a linear problem in the current increments of the fitting parameters, the solution to this ill-conditioned problem was found by modifying the original algorithm by obtaining the required algebraic solution by the use of singular value decomposition (SVD).[14,16] It turns out that SVD also fixes the roundoff problem and, in addition, it was found that it reduced the statistical uncertainties in the few first generations fitted parameters. The origin of the problems encountered with the method of normal equations lies in the fact that experimental data are not very sensitive to the contribution of higher generations.

B. Maximum entropy

The abovementioned nonlinear least squares method allows, in principle, the determination of one solution among the infinite feasible set of solutions reproducing the experimental data. A better restricted set of solutions, within the uncertainties arising from the intrinsic noise conforming to the single-photon timing techniques, can be extracted by using the MEM. This set of solutions has to verify the sample decay law [Eq. (5)] which can be rewritten as

$$\rho_b^\Omega(\lambda,t) = \sum_{n=1}^{\infty} p_n(\lambda) g_n(t), \tag{7}$$

where p_n is the nth generation molecule contribution to the overall decay.

It has been shown[17] that the best choice of the entropy (S), which should be free of artifacts introduced by numerical inversion of the above equation, is the Shannon–Jaynes entropy function defined (where the summation is truncated to a maximum allowed generation number n_{max}) as:

$$S = \sum_{n=1}^{n_{max}} p_n - m_n - p_n \log \frac{p_n}{m_n}. \tag{8}$$

It is then possible to recover a preferred solution within the ones of the feasible set. m_n is the starting model, and assumed as equiprobable for each generation of energy migration which is, in the absence of any information about the final solution, the lowest level hypothesis.

Since we are not working with a pure excitation δ-pulse function, the collected data are a convolution product of the impulse fluorescence decay by the instrumental response function. In the case where pure exponential fluorescence decays are assumed, recurrent iterative algorithms can be used in order to increase the data processing rate.[18] As no such iterative formula exists for the $g_n(t)$ function [Eq. (2)], it was necessary to use numerical integrations for each elemental reconvolution. Nevertheless, it should be noted that each of these elementary reconvolutions, corresponding to each energy migration step n value (although largely computer time consuming) is performed only once. Thus, a $\mathbf{G}_{kn}$ matrix is built in which each of its columns represent the time dependence of each successive photon migration step. This matrix remained unchanged during MEM processing. Thus, with such a linear system $\mathbf{I}_k = \mathbf{G}_{kn} \times \mathbf{p}_n$ the aim of MEM will be to increase the contrast of the $\mathbf{p}_n$ vector coordinate profile in the generation number space with respect to the minimization to an acceptable value of the quadratic difference in the time space between the weighted experimental and the reconvoluted curves. The MEMSYS5 (MEDC Ltd, Cambridge, U.K.) library of subroutines was used in a specifically modified FORTRAN 77 program.[19]

VI. RESULTS AND DISCUSSION

A. Data analysis

The main goal of this work is to provide an experimental test of the proposed stochastic theory of molecular radiative transport. As already discussed in Sec. V, the experimental recovered parameters to be confronted with the theoretical predictions were obtained by applying either a NLLS or a MEM data analysis procedure to the measured SPT fluorescence decays. Given the experimental recorded emission, one is left with fitting the data with the decay law rewritten as Eq. (7), truncated to a predetermined fixed number of generations. This number was always 30 for data analysis using MEM. For the NLLS, this number was smaller, usually from 6 to 15 terms, depending on the relative importance of the reabsorption process. It was found that MEM is superior to NLLS since it is able to discriminate from the experimen-

tal data the terms that do not contribute appreciably to the evaluation of the fitting function—if the experimental data are not very sensitive to the last generations contribution to the detected decay, then MEM drives the corresponding fitted parameters to zero while NLLS (after a critical number of parameters) is unable to do that, thus effectively precluding a good fit. Nevertheless, the significant parameters obtained from both methods were found to be in close agreement.

The cross usage of the two independent NLLS and MEM methods was important, as the data analysis of reabsorption distorted emission decays is an ill-conditioned numerical problem due to the necessity of using a high number of fitting parameters (identical to the number of generations considered). The agreement between the results from the two independent analysis procedures confirms that our recovered parameters are free of numerical artifacts. In the following discussion, we will indifferently use results obtained either from MEM or from NLLS and will concentrate solely on their comparison with MC predictions.

An additional point deserves to be mentioned. In Eqs. (5) and (7), the molecular, reabsorption free, decay parameter Γ was not used as a fitting parameter. This parameter was estimated from a single exponential analysis of the fluorescence decay obtained for a very dilute sample (5×10^{-7} M). The computed intrinsic decay lifetime was $\tau_0 = 4.34 \pm 0.04$ ns, and this value compares favorably with the value of 4.37 ns found in the literature for the zwitterionic form of the dye.[20] This value is then used as a fixed parameter in the analysis of the concentrated media data.

To be able to compare the MC predictions with the experimental results, one should first note that the data analysis of the decay according to Eq. (7) does not give the absolute value of the $p_n(\lambda)$ probabilities. The recovered parameters are related to these probabilities by a constant unknown parameter directly proportional to the overall number of counts recorded for the LUDOX scatterer. This effectively precludes a direct comparison of these probabilities but one can compare instead the relative contribution of each individual generation to the overall detected decay at each particular wavelength $\Theta_n^\Omega(\lambda)$:

$$\Theta_n^\Omega(\lambda) = \frac{\int p_n(\lambda) g_n(t) dt}{\int \Sigma_{n=1}^\infty p_n(\lambda) g_n(t) dt} = \frac{p_n(\lambda)}{\Sigma_{n=1}^\infty p_n(\lambda)} \quad (9)$$

which has the additional advantage of having a direct physical meaning. Another tested parameter is the mean excitation decay lifetime:

$$\tau^\Omega(\lambda) = \frac{\int_0^\infty t \rho_b^\Omega(\lambda, t) dt}{\int_0^\infty \rho_b^\Omega(\lambda, t) dt} = \left(\frac{\Sigma_{n=1}^\infty n p_n(\lambda)}{\Sigma_{n=1}^\infty p_n(\lambda)} \right) \tau_0$$

$$= \left(\sum_{n=1}^\infty n \Theta_n^\Omega(\lambda) \right) \tau_0. \quad (10)$$

B. Front-face geometry

Some experimental results obtained for a front-face geometry defined as having angles α' and β' (angle between the optical collection direction and the cell wall—Fig. 2 in Ref. 3) as 30° and 60°, respectively, are now presented. A
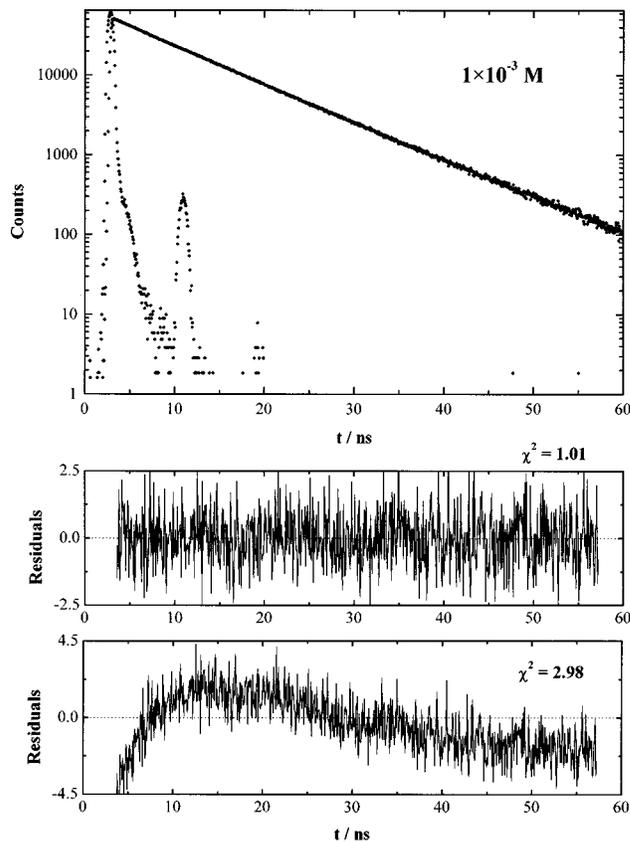

FIG. 3. Fluorescence decay of a 10^{-3} M solution of rhodamine 101 at room temperature in a front-face geometry ($\alpha' = 30°$, $\beta' = 60°$). Excitation wavelength was 319 nm while emission wavelength was 650 nm. The average lifetime is 8.95 ns. The fit to Eq. (7), with the lifetime fixed at the dilute solution experimental value, 4.34 ns, is quite good (main plot, upper residuals plot and reduced chi-squared value) while the fit to a single exponential is poor (lower residuals plot and reduced chi-squared value).

typical result obtained for a 10^{-3} M solution of rhodamine 101 at room temperature is shown in Fig. 3. The average excitation decay lifetime is 8.95 ns, slightly higher than twice the reabsorption free value. As one can see from the upper residuals plot and reduced chi-squared value, the fit to the radiative transport decay model [Eq. (5)] is quite good while the fit to a single exponential results in a nonrandom residual distribution with a considerably higher chi-squared statistic. A more critical test to the adequacy of Eq. (5) to describe reabsorption distorted fluorescence decays is provided by Fig. 4. In this figure the MC theoretical predictions and the experimental values of the relative contribution to the detected decay as a function of both the concentration and the emission wavelength are compared. A very good agreement between experiment and MC integration results is apparent. The upper plot depicts the influence of the wavelength for a 10^{-3} M solution excited at 294 nm. The theoretical predictions adequately explain the observed experimental trend; with the increase of reabsorption at the detection wavelength [going from 650 nm ($\varepsilon \approx 0$) to 580 nm ($\varepsilon = 9.6 \times 10^4$ M^{-1} cm^{-1})], the contribution of generations other than the first decreases. This effect can be understood as follows: For front-face detection and following excitation there is a progressively deeper penetration of excitation into
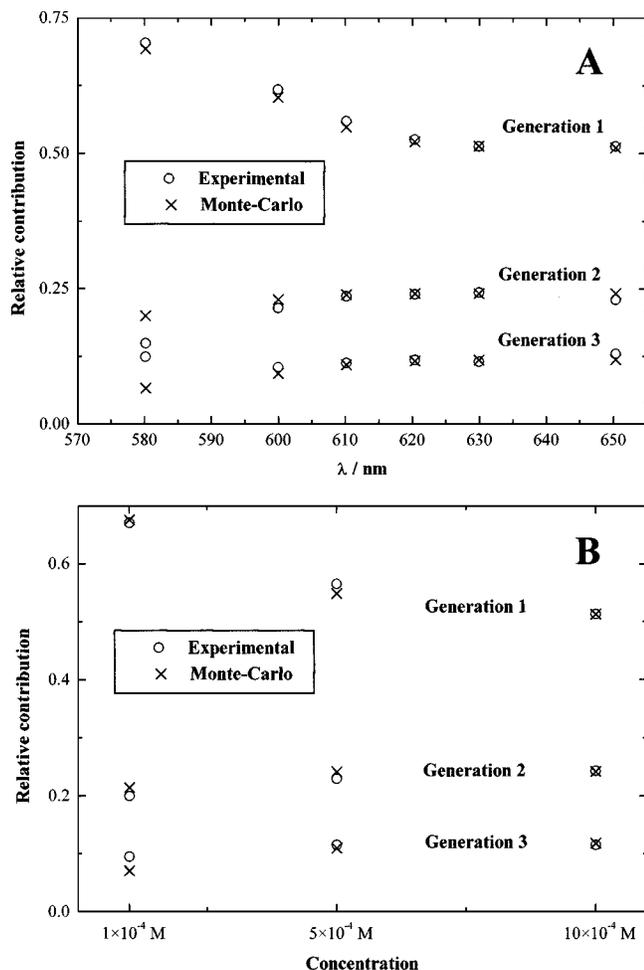
FIG. 4. Comparison between experimental and three-dimensional MC simulation predictions for the relative contributions to overall fluorescence decays as a function of the emission wavelength and concentration. Front-face ($\alpha' = 30°$, $\beta' = 60°$) viewing of a $1 \times 1 \times 3$ cm solution enclosure excited at 294 nm. (A) Influence of the emission wavelength for a 10^{-3} M solution. (B) Influence of the concentration for a 630 nm fixed detection wavelength.

FIG. 5. Comparison of experimental and three-dimensional MC predicted average lifetimes of rhodamine 101 for front-face geometry ($\alpha' = 30°$, $\beta' = 60°$). (A) Influence of the concentration and emission wavelength for a fixed 294 nm excitation. (B) Influence of excitation wavelength for a 10^{-3} M solution.

the interior of the sample cell. This means that the *n*th generation is farther away from the cell wall probed by the detection system when compared to the precedent generation. For wavelengths greater than the absorption cutoff, the emitted light is not reabsorbed, and all generations contribute to the observed decay, their relative importance being dictated only by the relative number of the *n*th generation molecules located inside the solid angle subtended by detection. On the other hand, for wavelengths in the overlap region, there will be a selective attenuation of the emission—the higher the generation, the higher the average pathlength that light must travel inside the cell in order to be detected and, therefore, the stronger the attenuation owing to reabsorption. In the limiting case of very strong absorption, only the excited molecules located very near the wall will contribute to the observed decay. As can be seen in Fig. 4, the effect is important, the relative weight of the directly excited molecules changing from 51% to 70% when going from essentially reabsorption-free conditions to strong reabsorption at 580 nm.

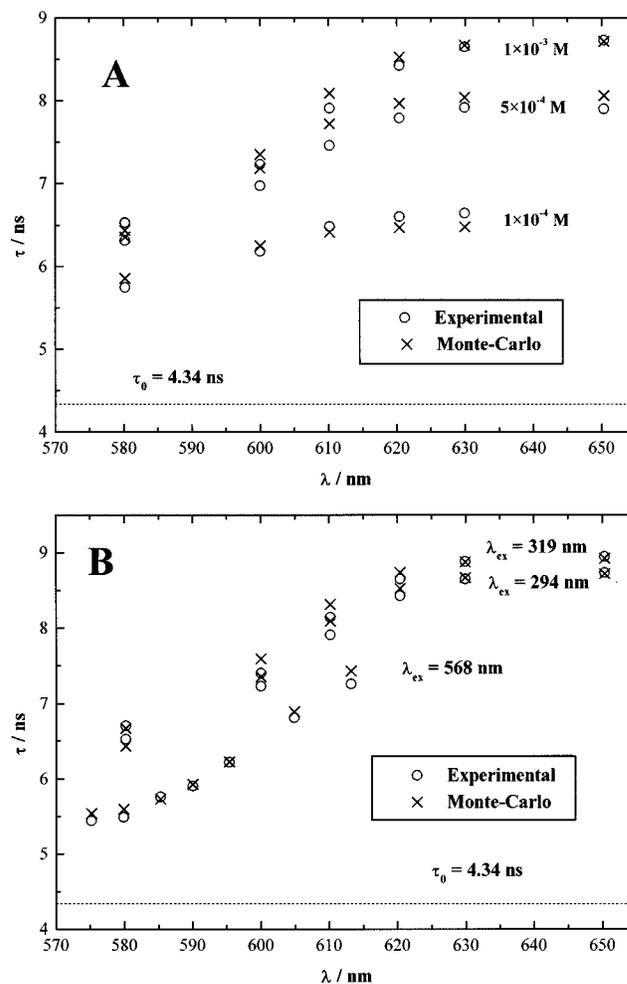The lower plot in Fig. 4 shows the effect of changing the

concentration while keeping the excitation and emission wavelengths constant at 294 and 630 nm, respectively. As expected, an increased concentration leads to an increased importance of radiative migration, thus diminishing the relative weight of the directly excited molecules.

Figure 5 shows results more directly connected to the usual experimental parameters. In the upper plot of Fig. 5, mean fluorescence lifetimes, computed according to Eq. (10) as a function of both concentration and detection wavelength for a 294 nm excitation wavelength, are presented. The agreement between the MC results and the experimental results is again very good and this figure shows well-established trends for radiative transport, namely that the higher the concentration the higher the importance of radiative migration, and consequently the higher the overall mean lifetimes. It is shown that, for rhodamine like molecules, concentrations as common as 10^{-4} M give rise to lifetimes significantly higher than the dilute reabsorption free counterparts—the increase from the intrinsic lifetime varies from 32% at 580 nm to 53% at 630 nm. The influence of the emission wavelength dependence is directly related to the discussion of Fig. 4—to a decrease in the contribution of

J. Chem. Phys., Vol. 110, No. 3, 15 January 1999

Nunes Pereira *et al.*   1607

higher generations to the decay (which, on the average will decay at higher times) corresponds of course to a faster decay with smaller lifetime. The emission wavelength dependence is very strong as one can see for the data of the 10^{-3} M solution—when going from 580 to 650 nm the average lifetime changes from 6.53 to 8.74 ns, corresponding to a 34% relative increase.

The lower plot of Fig. 5 shows that the excitation wavelength can also have a very strong influence on the mean fluorescence lifetimes. In this figure results obtained for a 10^{-3} M solution excited at three different wavelengths: 319 nm ($\varepsilon = 1.0 \times 10^4$ M^{-1} cm^{-1}), 294 nm ($\varepsilon = 1.6 \times 10^4$ M^{-1} cm^{-1}) and 568 nm ($\varepsilon = 1.1 \times 10^5$ M^{-1} cm^{-1}) are presented. By varying the excitation wavelength, the relevant physical quantity that is changed is the penetration of external excitation into the sample cell; the first two wavelengths correspond to a roughly equal penetration, while the latter corresponds to a much smaller penetration of excitation, since $\varepsilon_{568\ nm}$ is roughly ten times higher. To discuss the effect of changing the excitation wavelength let us first briefly mention the effect of changing concentration. The increase in concentration has a twofold effect on the radiative transport process. It leads to higher optical densities at both excitation and emission wavelengths. The effect for the former wavelength is to reduce the penetration of external laser excitation into the sample cell, primarily excited molecules being thus located nearer the cell's wall. The effect for the latter wavelength is to reduce the mean optical path of the emitted photons prior to reabsorption, thus effectively reducing excitation spread when going from one generation to the next, and increasing average reabsorption probabilities in finite volume cells. The first effect tends to reduce the influence of radiative transport since excitation nearer the cell wall will increase escape probabilities (solely in the direction of front-face detection) while the second effect tends to increase the importance of radiative migration because reabsorption probabilities for the same pathlength will increase. The second effect dominates and therefore, as the result of an increased concentration, higher decay lifetimes are observed, as can be seen in Fig. 5. On the other hand, variation of λ_{ex} changes the optical density at the excitation wavelength but not at the emission wavelength. If the excitation optical density is increased while concentration remains constant, then the primarily excited molecules will become located closer to the excitation side. Although the excitation spreading induced by reabsorption does not change, the overall importance of radiative migration decreases, because mean escape probabilities from the sample cell will increase. The picture is particularly clear if one considers the spatial distribution functions for several generations of excited species, not accessible experimentally but easily computed from the described MC simulation procedure [see for instance Fig. 4 in Ref. 3].

While the emission wavelength dependence of the mean reabsorption distorted lifetimes is well known, their dependence on the excitation wavelength was not, to the best of our knowledge, fully recognized in the literature prior to our previous discussion.[3,21] Figure 5 clearly shows the relevance of a precise statement of the excitation conditions whenever
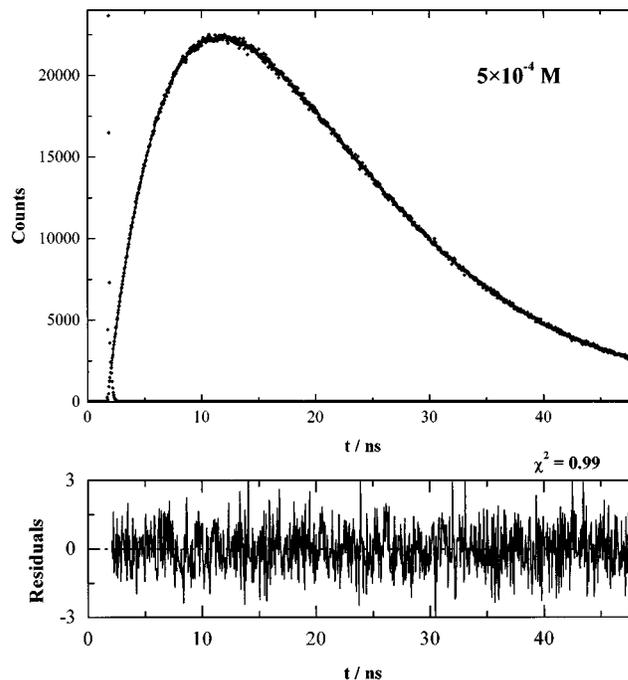

FIG. 6. Fluorescence decay of a 5×10^{-4} M solution of rhodamine 101 at room temperature in a right-angle geometry. Excitation wavelength was 300 nm and emission wavelength was 590 nm. The average lifetime is 19.48 ns. The fit to Eq. (7), with the lifetime fixed at the dilute solution experimental value, 4.34 ns, is quite good.

presenting emission decays for which reabsorption effects are likely.

C. Right-angle geometry

In Fig. 6 a fluorescence decay recorded for a 5×10^{-4} M solution of rhodamine 101 in a right-angle geometry, with the detection optics focusing on the middle of the cell wall, is presented. Excitation wavelength was 300 nm and emission wavelength was 590 nm. The fit to Eq. (5) is quite good, as one can judge from the reduced chi-squared value and from the weighted residuals distribution. The average lifetime is 19.48 ns, more than four times the reabsorption-free value. This high value is mainly the result of a long and clear rise time in the decay. For the right-angle geometry, external excitation impinges in the middle of the cell wall facing the laser beam (Fig. 1). This means in practice that, for the 1 cm conventional square cell used, the emission from the directly excited molecules will have to pass through a 0.5 cm absorbing pathlength before being detected. When the optical density at the selected wavelength is high enough, practically all photons emitted from the first generation molecules are reabsorbed inside the sample cell thus having a negligible contribution to the decay. Nevertheless, as reabsorption induces excitation spread in the sample cell, the indirectly excited molecules will be nearer the detection path, and so will contribute to the decay. Since the indirectly excited molecules decay on average at longer times [the maximum decay of the nth generation emission will occur at $(n-1)\tau_0$] what is detected is an emission buildup resulting in the observed rise time. For emission wavelengths where reabsorption over the 0.5 cm is incomplete, directly excited molecules contribute

to the overall decay and the contribution of the indirectly excited ones will not suffice to produce a rise time.

For the previously reported front-face geometry, excitation is always walking away from the cell wall, and the average pathlength for reabsorption is always increasing with generation number. Since, as one goes from one generation to the next, the number of excited molecules decreases because some of the excitation can escape, the contribution to the observed decay from one generation is always higher than the contribution from the next one. So, no matter what detection wavelength we select, a rise time is never observed.

Although experimental evidence for rise times has never, to the best of our knowledge, been unambiguously identified with radiative transport in the literature prior to our preliminary report,[22] some experimental results nevertheless exist. Reabsorption is probably the cause of the rise-times observed in some fluorescence decays of rhodamine B[23] and rhodamine 575.[24]

Figure 7 compares the MC predictions and the experimentally observed values for the relative contributions to the detected decays as a function of both the emission wavelength and of detection position in the experimental cell for the first three generations of excited molecules. These results were obtained for a 10^{-4} M solution enclosure excited at 300 nm and positions 1, 2 and 3 correspond approximately to optical focusing at 0.25, 0.50 and 0.75 cm, distances measured from the cell wall facing excitation. The experimental decays were recorded using a simple black paper mask with a 5 mm diameter hole at the appropriate positions. The upper plot analyzes the influence of the emission wavelength while the lower one addresses the problem of the detection coordinate. Figure 7(A) shows the 580–590 nm region as a transition one. For smaller wavelengths, first generation molecules will contribute less than second or third generation ones while for higher wavelengths the situation is reversed, with first generation molecules contributing significantly more than the remaining ones. This transition is associated with the appearance of rise times in the fluorescence decays recorded for wavelengths lower than $\simeq 585$ nm. In the red part of the spectrum no rise time is detected since reabsorption is weak and the directly excited molecules will account for approximately 60% of the overall decay.

The lower part of Fig. 7 corresponds to a fixed 590 nm detection wavelength and the observed differences cannot therefore be attributed to a selective optical density dependent reabsorption. On physical grounds, there are two factors affecting the relative importance of the several generations of excited molecules. The first one is a differential attenuation of the emission arising from different generations since, owing to different spatial distributions that lead to a different photon pathlength before escape. The second is just a question of how many species from different generations exist in the finite volume subtended by the detection solid angle. The Lambert–Beer law is strongly nonlinear in the pathlength and many more first generation molecules are near the cell wall facing excitation than in the central part of the cell. Owing to excitation migration, this difference will be less pronounced for the second generation, and even less for the
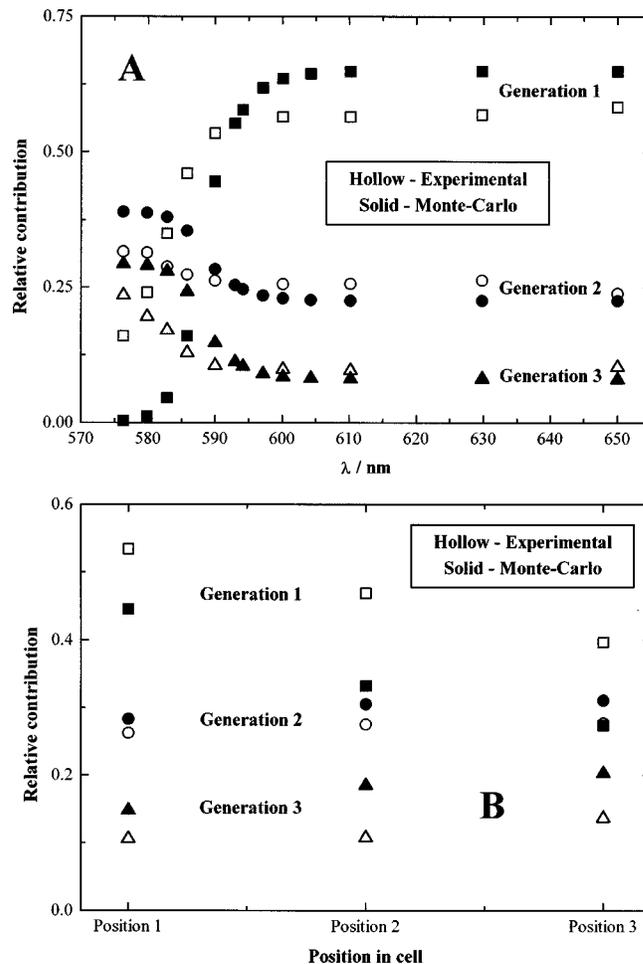

FIG. 7. Comparison between experimental and three-dimensional MC simulation predictions for the relative contributions to overall fluorescence decays as a function of the emission wavelength and of the detection position in the experimental cell for the first three generations of excited molecules. Right-angle viewing of a $1\times1\times3$ cm 10^{-4} M solution enclosure excited at 300 nm. (A) Influence of the detection wavelength with detection fixed at position 1. (B) Influence of the detection coordinate with emission wavelength fixed at 590 nm.

third, etc. As a result, Fig. 7 shows that the relative contribution of the directly excited molecules will be smaller the farther the recording point is from the cell wall facing external excitation. Again, the central key to understanding the excitation dynamics is the spatial evolution of the excitation corresponding to the different generations.

From Fig. 14 of Ref. 3 one sees that, for the 10^{-4} M conditions of Fig. 7, external excitation is able to reach the cell wall opposite the one facing the 300 nm laser beam. This means that, no matter what coordinates are selected to detect fluorescence at right-angle, we are always able to see the emission coming from the directly excited molecules as long as reabsorption is low enough (in agreement with Fig. 7). However, if penetration is lowered by increasing either concentration or absorption coefficient at excitation wavelength, there will be regions of the cell with no directly excited molecules. Sufficiently far from the cell wall facing detection, the only excitation present will be the result of radiative transport and, if one focuses on the detection in these regions, we will always see a rise time even for reabsorption-
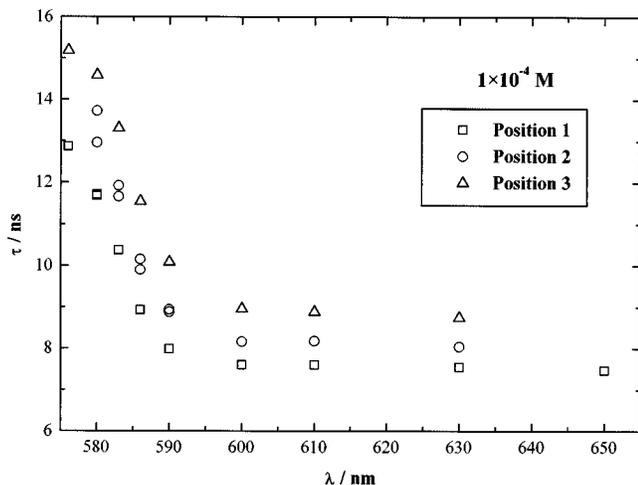
FIG. 8. Experimental average lifetimes of rhodamine 101 for right-angle detection as a function of detection coordinate for a 1×10^{-4} M solution.
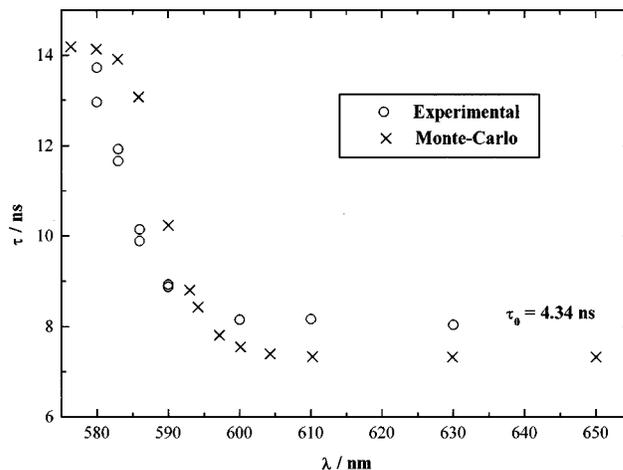

FIG. 9. Comparison of experimental and three-dimensional MC predicted average lifetimes of rhodamine 101 for a right-angle geometry as a function of emission wavelength for a 1×10^{-4} M solution excited at 300 nm. Detection coordinates corresponding to position number 2 in cell.

free wavelengths. This was experimentally verified[25] and confirms the authors previous predictions.[3]

Figure 8 shows some experimental mean fluorescence lifetimes obtained for a 300 nm excitation of a 1×10^{-4} M solution for the previously defined detection positions 1, 2 and 3. All other factors being constant, the farther the fluorescence is collected from the cell wall exposed to direct excitation, the higher the lifetime since we are effectively minimizing the contribution of first generation molecules.

From the data shown in Figs. 7 and 8, a very clear picture of reabsorption distorted data emerges as being characterized by a lifetime surface topography spatially resolved in the sample cell. This spatially resolved fluorescence kinetics is a direct consequence of the existence of inhomogeneous spatial distribution functions for the several generations of excited species, which are probed with different statistical weights, depending on the optical density at the chosen emission wavelength.

Finally, Fig. 9 compares the mean lifetimes predicted by a MC integration of the stochastic escape probabilities with the experimentally obtained values for a 1×10^{-4} M solution corresponding to the middle position. In light of the dependence of the observed decay from the experimental detection spot, one can consider the agreement quite reasonable.

The fact that the agreement between experimental data and theoretical predictions is not as good for right-angle as for front-face is understandable if one considers the critical dependence of the results on the alignment of the optical collecting system for this geometry, especially for concentrated solutions. For front-face, the adjustment of the detection is straightforward; all one has to do is to adjust the collecting optics so that one sees the maximum count rate of the fluorescence emission. Since, in this last geometry, excitation is moving away from the face of the cell probed by detection, this ensures that the collecting optics is focused on the impinging excitation laser spot and experimentally mimics the approximations used for the MC simulations. For right-angle the alignment is more difficult since, as the spatial distribution of the first generation molecules is strongly inhomogeneous, the experimental decays become very sen-

sitive to the precise focusing of the detection spot in the sample cell. In fact, it was verified that changing the position of the sample cell over 1 or 2 mm along the normal coordinate to the detection system could change the decay significantly. For this geometry there are two interconnected aspects that are important. First of all, even for concentrations as low as 10^{-4} M, the excited species spatial distributions can be strongly inhomogeneous on a scale of 1–5 mm, provided the excitation optical density is high enough. Although the fluorescence emission coming from a point along the optical axis of the collection system will be correctly imaged into the monochromator entrance slit, the off-axis emission can be partially cutoff by the field stop or other stops in the system. Due to this *vignetting* there can be a gradual loss of light as we move farther off axis and this can make the MC assumption of a 5 mm diameter effective cylinder a crude one. A second aspect may also be important: Even for a perfect on-axis illumination of the monochromator slit, the collection optics efficiency may be generation dependent. In fact, the closer the emission is to the first lens of the optics, the greater the flux density, because the solid angle of the transmitted light cone increases. So, in a first order approximation, this change of the detected solid angle can be important if the spatial spread of the excitation inside the sample is not much smaller than the distance between the experimental cell and the first lens of the collection optics system. MC simulations, considering a position dependent transmitted on-axis solid angle inside the effective cylinder for detection, showed that this effect was not important for our experimental apparatus optical setup.

VII. SUMMARY AND CONCLUSIONS

Following parts I and II of this series, a detailed experimental test of the validity of the proposed treatment of molecular radiative transport in optical dense and nondiffusing media is presented. The probabilistic MC integration of the theoretical expressions for the mean escape probabilities is validated by confronting the predictions for the time-

resolved fluorescence intensity decays with experimental results obtained in two common configurations: front-face and right-angle detection, both using a standard square 1 cm cuvette. The quantities compared were the relative contributions to the overall detected decays and the mean emission decay times. A good general agreement was found, deviations between predicted and experimental results being somewhat larger for the right-angle case.

It can be concluded that the developed theory for molecular radiative transport associated with the proposed MC integration procedure accurately describes the quantitative experimental results. In particular, it accounts for the well-known dependence of the observed decays on the concentration and emission wavelengths. It also accounts for two non-trivial effects: the dependence on the excitation wavelength via the change of the overall importance of radiative transport, and the possible existence of rise times associated with the fluorescence decays recorded in a right-angle geometry. It must be emphasized that the key for understanding all aspects of reabsorption distorted data is the visualization of the spatial distribution functions of the different generations of excited species. These distribution functions, although easily obtained by MC simulation of the photon trajectories, are not experimentally accessible, since all generations contribute to the decay in an inseparable manner.

In order to evaluate the number of reliable parameters extractable from the analysis of experimental SPT data, a detailed study was conducted on synthetic decays. From the MC integrated mean escape probabilities, several synthetic fluorescence decays were generated: the δ-decay law was convoluted with the experimental instrumental response function and, for each data channel, a Poisson random deviate was generated.[14] These synthetic decays were then analyzed and the fitted parameters were compared with the MC initial ones. From a detailed analysis of the results, several general conclusions could be drawn. First, mean decays lifetimes were always recovered with an accuracy better than 1%. The recovery of the parameters pertaining to each generation is delicate, since experimental data are not sensible to small contributions. It was found that mean escape probabilities were recovered with better than 5% accuracy as long as the individual contribution of the generation to the decay was at least 20%. Nevertheless, in the worst case scenario, for generations contributing between 5% and 20%, the difference between simulation and recovered parameters was at most 10%. For generations with less than a 5% contribution, numerical instabilities were found, the accuracy of the obtained parameters becoming strongly dependent on the overall number of counts recorded for the decay. In practice, this is not an important limitation, owing to the reduced importance of these generations to the emission data. For rhodamine 101 with concentrations in the experimental range used, one can expect to reliably obtain between three and eight contributing terms, depending on the conditions.

Although molecular radiative transport is a general phenomenon, its importance in each experimental system depends on molecular parameters: absorption–emission spectral overlap, fluorescence quantum yield, and absorption coefficients in the overlap region. Moreover, whenever present, the fluorescence data become dependent on macroscopic details such as the concentration and tree size of the sample solution and on several experimental details such as the chosen geometry, the particular wavelength values used to excite and detect emission and the probed position inside the experimental cell.

[1] M. N. Berberan-Santos, E. J. Nunes Pereira, and J. M. G. Martinho, J. Chem. Phys. **103**, 3022 (1995).

[2] M. N. Berberan-Santos, E. J. Nunes Pereira, and J. M. G. Martinho, J. Chem. Phys. **107**, 10480 (1997).

[3] E. J. Nunes Pereira, M. N. Berberan-Santos, and J. M. G. Martinho, J. Chem. Phys. **104**, 8950 (1996).

[4] J. M. G. Martinho, A. L. Maçanita, and M. N. Berberan-Santos, J. Chem. Phys. **90**, 53 (1989).

[5] Th. Förster, Ann. Phys. (Leipzig) **2**, 55 (1948).

[6] J. Ferguson and A. W. H. Mau, Chem. Phys. Lett. **17**, 543 (1972).

[7] (a) F. López Arbeloa, I. Urreche Aguirresacona, and I. López Arbeloa, Chem. Phys. **130**, 371 (1988); (b) F. López Arbeloa, T. López Arbeloa, M. J. Tapia Estévez, and I. López Arbeloa, J. Phys. Chem. **95**, 2203 (1991).

[8] D. V. O'Connor and D. Phillips, *Time-correlated Single Photon Counting* (Academic, London, 1984).

[9] J. N. Demas and G. A. Crosby, J. Phys. Chem. **75**, 991 (1971).

[10] J. Olmsted III, J. Phys. Chem. **83**, 2581 (1979).

[11] D. Magde, J. B. Brannon, T. L. Cremers, and J. Olmsted III, J. Phys. Chem. **83**, 696 (1979).

[12] (a) D. F. Eaton, J. Photochem. Photobiol., B **2**, 523 (1988); (b) T. Karstens and K. Kobs, J. Phys. Chem. **84**, 1871 (1980).

[13] J. Arden-Jacob, N. J. Marx, and K. H. Drexhage, J. Fluoresc. **7**, 91S (1997).

[14] W. H. Press, S. A. Teukolsky, W. T. Vetterling, and B. P. Flannery, *Numerical Recipes*, 2nd ed. (Cambrige University Press, Cambridge, 1992).

[15] D. W. Marquardt, J. Soc. Ind. Appl. Math. **11**, 431 (1963).

[16] (a) Å. Björck, *Numerical Methods for Least Squares Problems* (SIAM Society for Industrial and Applied Mathematics, Philadelphia, 1996); (b) C. L. Lawson and R. J. Hanson, *Solving Least Squares Problems* (SIAM Society for Industrial and Applied Mathematics, Philadelphia, 1995).

[17] A. K. Livesey and J. C. Brochon, Biophys. J. **52**, 693 (1987).

[18] (a) Ph. Wahl, Biophys. Chem. **10**, 91 (1979); (b) A. Grindvald and I. Z. Steinberg, Anal. Biochem. **59**, 583 (1974); (c) Z. Bajzer, A. Zelic, and F. G. Prendergast, Biophys. J. **69**, 1148 (1995).

[19] M. Vincent, J. Gallay, and A. Demchenko, J. Phys. Chem. **99**, 14931 (1995).

[20] J. Karpiuk, Z. R. Grabowski, and F. C. De Schryver, J. Phys. Chem. **98**, 3247 (1994).

[21] E. J. Nunes Pereira, M. N. Berberan-Santos, and J. M. G. Martinho, J. Lumin. **63**, 259 (1995).

[22] M. N. Berberan-Santos, E. J. Nunes Pereira, and J. M. G. Martinho, J. Fluoresc. **7**, 119S (1997).

[23] Y. Sakai, M. Kawahigashi, T. Minami, T. Inoue, and S. Hirayama, J. Lumin. **42**, 317 (1989).

[24] (a) J. S. Batchelder, A. H. Zewail, and T. Cole, Appl. Opt. **18**, 3090 (1979); (b) *ibid.* **20**, 3733 (1980).

[25] E. J. Nunes Pereira, M. N. Berberan-Santos, and J. M. G. Martinho (unpublished).